



23 European Conference on Fracture - ECF23

Wear and corrosion behavior of 18Ni-300 maraging steel produced by laser-based powder bed fusion and conventional route

Pietro Tonolini^{a*}, Luca Marchini^a, Lorenzo Montesano^a, Marcello Gelfi^a, Annalisa Pola^a

^a *University of Brescia, Department of Mechanical and Industrial Engineering, via Brancaleoni, 38056
Brescia, Italy*

Abstract

Maraging steels such as 18Ni-300 (1.2709) are characterized by high yield and tensile strength together with good toughness making them interesting materials for aerospace, automotive and tooling sectors as well as for bearing gears parts. The low carbon martensite matrix combined with the nanosized intermetallic precipitates are responsible for the peculiar mechanical properties. Thanks to the very low carbon content, these steels are easily weldable and therefore suitable for additive manufacturing (AM) techniques, such as laser-based powder bed fusion (LPBF). Indeed, this technique was recently adopted in tooling and molding industry to produce inserts with conformal cooling channels capable to improve inserts and cores lifetime enhancing productivity. These types of components usually undergo severe stress conditions, wear phenomena and even aggressive environments.

This work aims at comparing the tribological and corrosion behaviour of 1.2709 maraging steel samples produced by both forging and LPBF technique. Conventional samples were investigated after solution annealing and aging treatment while AM samples were directly aged. Aging parameters were chosen to achieve the same hardness values for both the production conditions. Samples sliding wear behaviour was investigated through pin-on-disc tests using 100Cr6 steel ball as counterpart (ASTM G99) at three different sliding velocities, while potentiodynamic polarization measurements (ASTM G3) were conducted in 3.5 wt % NaCl solution.

Microstructural analyses and hardness measurements were carried out on as-aged samples. The corrosion damage and the wear mechanism were investigated by means of scanning electron microscope (SEM). For the considered heat treatment, results show only small differences on the wear and corrosion behaviors between forged and AM samples, despite differences in the microstructural morphology, demonstrating the reliability of AM components.

© 2022 The Authors. Published by Elsevier B.V.

This is an open access article under the CC BY-NC-ND license (<https://creativecommons.org/licenses/by-nc-nd/4.0>)

Peer-review under responsibility of the scientific committee of the 23 European Conference on Fracture – ECF23

Keywords: Maraging steel; Wear; Corrosion

* Corresponding author. Tel.: +390303715826.

E-mail address: p.tonolini002@unibs.it

1. Introduction

Maraging steels such as 18Ni-300 (1.2709) are characterized by high yield and tensile strength together with good toughness (Handbook 1993). The low carbon martensite matrix formed by cooling from the high Ni content-Fe solid solution, combined with the precipitation strengthening of nanosized intermetallics, such as Ni₃Ti (Pereloma et al. 2004), Ni₃Mo (Rao 2006), NiAl (Schnitzer et al. 2010), Ni₃Al (Shin, Jeong and Lee 2015), Fe₂Mo (Vasudevan, Kim and Wayman 1990), etc., obtained after aging at temperature of about 450-550 °C, are responsible for the peculiar mechanical properties. In fact, maraging steels are interesting materials for aerospace (Narayana Murty and Sharma 2022), automotive (Pennings, Hatanaka and Crebolder 2015) and tooling (Ferreira et al. 2021) sectors as well as for bearing gears parts (Kim et al. 1986). Furthermore, maraging steels present good dimensional stability and low coefficient of thermal expansion (Handbook 1993) that together with the very low content of interstitials alloying elements make this class of steels easy to weld (Lang and Kenyon 1971) and therefore suitable for additive manufacturing (AM) techniques, such as laser-based powder bed fusion (LPBF), also known as selective laser melting (SLM).

LPBF is a 3D printing method that uses a powder bed of the chosen alloy and a laser source to selectively melt successive layers of powder obtaining the subsequent building of near-net-shape 3D parts from input CAD data (ISO/ASTM 2019). Nowadays, different metallic powders can be processed via LPBF technique. The most investigated alloys in the literature are Al-based (Aboulkhair et al. 2019), Ti-based (Zhang and Attar 2016), Co-based (Sing et al. 2016), Ni-based (Elahinia et al. 2016) and Fe-based (Zitelli, Folgarait and Di Schino 2019). Optimized printing parameters permit to obtain very dense parts with comparable mechanical properties to those of components realized by conventional production route. For example, in the case of maraging steels, thanks to the extremely high cooling rates (up to 108 K/s (Jäggle et al. 2014)) typical of LPBF process that also promotes a sort of intrinsic solution heat treatment, the as-build parts develop a very fine cellular martensite microstructure, which only requires a final aging treatment to reach the mechanical properties of conventional manufactured parts (Casati et al. 2016). Furthermore, compared to forging process, LPBF technique allows much greater freedom of design and a lower need for subsequent machining operations, thus reducing material wastage. Indeed, this technique was recently adopted in tooling and molding industry to produce inserts with conformal cooling channels capable to improve inserts and cores lifetime, enhancing productivity. All these types of components usually undergo severe loads, wear phenomena and even aggressive environments. Thus, the aim of this work is to compare the wear and corrosion behavior of 18Ni-300 (1.2709) maraging steel produced by both AM technique and by conventional route.

2. Materials and methods

The maraging steels under investigation were industrially produced by Deutsche Edelstahlwerke Specialty Steel GmbH & Co. KG by both Additive Manufacturing techniques (AM) and conventional route (CR), consisting in the following steps: electric arc furnace melting, ladle furnace refinement, vacuum arc remelting and final forging.

The commercial powder namely Printdur® Powderfort (~1.2709) was chosen for building the AM samples. Concerning the particle size distribution, 3.4 vol.% of the powder is characterized by a diameter smaller than 20 µm, 45.6 vol.% smaller than 38 µm, and 98.2 vol.% smaller than 53 µm. The powder flow rate was 15.6 s/50g with an apparent density of 3.99 g/cm³. A commercially available laser-based powder bed fusion (LPBF) system was used to produce the maraging steel samples. The process parameters are confidential factory information that cannot be disclosed, as mentioned in other papers in the literature (Giovagnoli et al. 2021). AM samples are cylinders with a diameter of 57 mm and a height of 12 mm, manufactured, with the axis perpendicular to the building direction (BD).

The CR maraging steel was produced with the Cryodur®2709 commercial alloy. These samples were cut from a forged round bar with a diameter of 60 mm and machined to obtain the same dimensions of the AM samples.

Table 1 shows the mean chemical composition of the samples provided by the manufacturer and measured by optical emission spectroscopy.

Table 1 Samples mean chemical composition

Element (wt%)	C	Si	Mn	P	S	Cr	Mo	Ni	Co	Ti	N	O	Fe
AM	0.01	0.2	0.3	0.01	0.006	0.1	5	17.9	13.4	-	0.007	0.026	Bal.
CR	0.004	0.02	0.03	<0.003	0.0014	0.1	4.95	18.3	9.75	1.13	-	-	Bal.

The samples were heat treated to obtain the final mechanical properties. CR samples underwent solution treatment for 1 h at 820 °C, followed by air quenching and aging for 5 h and 30 min at 490 °C. Instead, only aging treatment was conducted on AM samples, holding the samples for 4 h at 490°C to promote the formation of precipitates (Casati et al. 2016). These heat treatment parameters were chosen on the base of manufacturer experience to achieve the same hardness for both AM and CR samples.

After heat treatment, all samples were machined to obtain discs with a diameter of 55 mm and a thickness of 10 mm. The flat surfaces were finished to a roughness of 0.4 μ m.

Microstructural characterization of aged samples was carried out after polishing up to a mirror finish and etching with modified Fry's reagent or Nital 4% (E407 2017). An optical microscope (Leica DMI 5000M) and a scanning electron microscope (LEO EVO 40, Zeiss) equipped with an energy dispersive spectroscopy microprobe (EDS, Oxford Instruments) were used for microstructural analysis. Furthermore, X-ray diffraction (XRD, Phoenix S.N. 01-2018) measurements were carried out to quantify the retained austenite in the samples, by using a Mo $k\alpha$ radiation ($\lambda = 0.7107 \text{ \AA}$), a voltage of 45 KV and a current of 35 mA, in according with the ASTM E975 standard.

Rockwell hardness (HRC) of samples was measured following ASTM E18 standard by means of a Rupac 500 Mra hardness tester and the mean value was calculated as the average of 5 indentations.

The wear behavior of aged maraging steel samples was evaluated with pin-on-disk (PoD) dry wear test by using a THT tribometer (CSM Instruments) in accordance with the ASTM G99 standard and adopting as counterpart a 6 mm diameter 100Cr6 steel ball. The effect of three different sliding velocities on the wear mechanism was investigated. Tests were performed at 22.5 cm/s, 50 cm/s and 62 cm/s, applying a constant load of 5 N, on a distance of 1260 meters. During the tests, the coefficient of friction (CoF) was continuously recorded while, at the end of each test, a stylus profilometer (TRIBOtechnic) was used to measure the wear track profile. At least three tests were carried out for each velocity and material condition and five wear track profile measurements were performed to calculate the mean value of the worn surface for each test. The wear rate was then calculated using the equation 1:

$$W = \frac{2 \pi r A}{F L} \quad (1)$$

where A is the average value of the worn surface (mm²), r is the radius of the wear tracks (i.e. 20 mm), F and L are the applied load (N) and the sliding distance (m) respectively.

To investigate the wear mechanisms, the worn surfaces (disc and counterpart) were analyzed by SEM-EDS technique at the end of each test.

The potentiodynamic polarization measurements (ASTM G3) were carried out at room temperature (25 °C) in a 3.5 wt % NaCl solution by means of a potentiostat (Model 7050 AMEL S.r.l.), by using a saturated calomel electrode (SCE) as reference electrode, two platinum wires as the counter-electrodes and the sample as working electrode. Samples were machined to fit into the sample holder that has an exposed circular surface of 5 mm in diameter. The specimens' surface was polished up to P1200 emery paper to remove any possible external oxide produced by the manufacturing process. The corrosion behavior of AM samples was investigated both on vertical (parallel to the BD) and horizontal (normal to the BD) section of the samples to identify the possible effect of the different orientation of the microstructure on the corrosion rate.

After 1 hour of samples immersion in the solution to stabilize the open circuit potential (Eoc), each test was performed at a scan rate of 0.25 mV/s from Eoc to Eoc - 300 mV (cathodic polarization) and return to Eoc and again from Eoc up to Eoc + 300 mV (anodic polarization). During each test, electrochemical data was automatically acquired to plot the potentiodynamic polarization curves. The corrosion current density and the corrosion potential values were extrapolated by Tafel method.

3. Results and discussion

Figure 1 displays the optical microscope images of aged AM samples after etching with Nital 4%. Notwithstanding the aging heat treatment, the overlapped elongated scan tracks typical of as-built AM parts can be recognized in the horizontal cross-section (Figure 1a) as also the semi-elliptical melt pools in the vertical cross-section (Figure 1b) whose width and depth depend on the adopted laser parameters and building strategy (Song et al. 2019). No porosity was detected suggesting the achievement of a fully dense parts. On the other hand, some unetched zones can be identified at the melt pool boundaries both vertical cross-section (Figure 1b) and in the horizontal (not presented here). According to the EDS analysis of Figure 1c, these zones correspond to positive segregations of Cr and Mo that form during solidification due to the partitioning of these elements into the last liquid that solidifies. This local enrichment of elements, typically located at cellular and dendritic boundaries but also at the boundaries of the scan tracks and melt pools, promotes the formation of retained austenite in AM maraging steel (Xu et al. 2018, Bai et al. 2019). In fact, despite Cr and Mo are ferrite stabilizer, their high concentration in the segregated zone locally decreases the martensite starting temperature (M_s) of steel to less than zero degree ($-43\text{ }^\circ\text{C}$), as calculated by the empirical equation proposed by Liu et al. (Liu et al. 2001), resulting in the stabilization of austenite at room temperature.

The aged AM microstructure at high magnification is shown in Figure 1d. As reported in other works (Yin et al. 2018, Casati et al. 2016, Bai et al. 2019), during the aging treatment, the very fine continuous cellular structure, typical of as-built parts, tends to blur with the increasing of holding time and temperature. At the same time the boundaries of the cells become non-continuous and irregular due to the precipitation of nano-sized Ni intermetallic phase and phase transformations can occur (e.g. formation of reverted austenite).

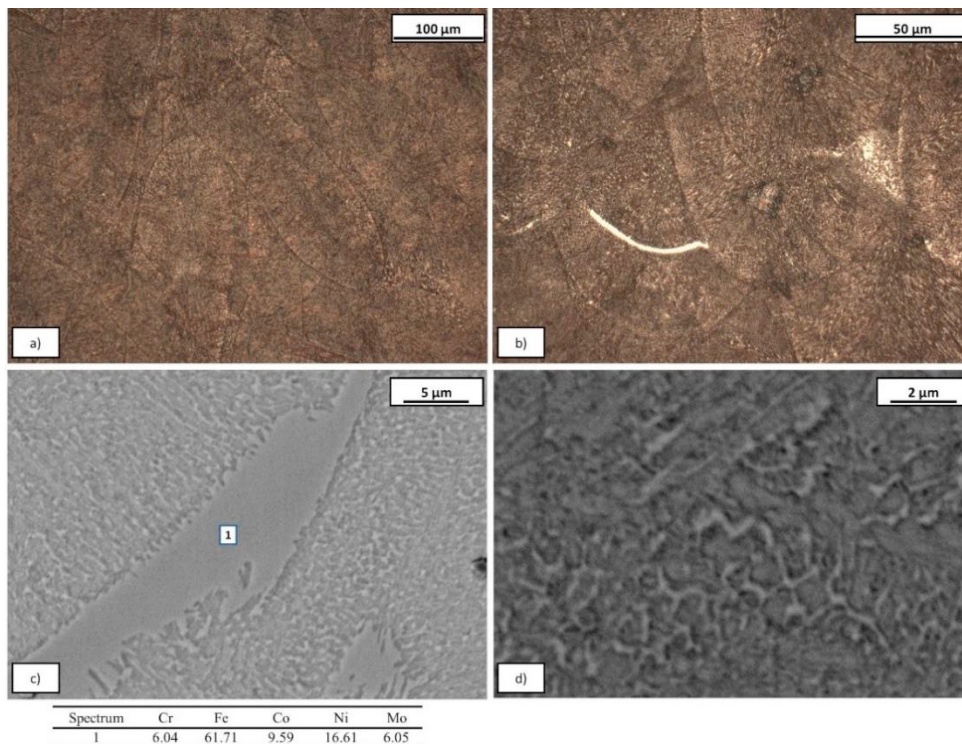


Figure 1 AM aged samples: a) horizontal and b) vertical cross-section; c) and d) SEM image and EDS analysis of AM vertical cross-section.

The microstructure of CR samples after solution treatment and aging is displayed in Figure 2. Samples etched with Nital 4% reveals packets or blocks of lath type martensite with very fine unetched boundaries that probably consist of reverse austenite (Fig. 2a). Instead, etching with modified Fry's reagent puts in evidence the different orientation of martensite blocks (Fig. 2b) (Morito et al. 2006).

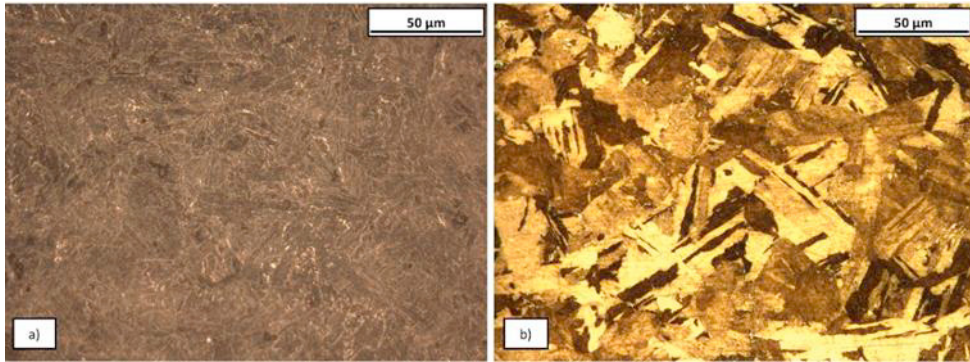


Figure 2 CR samples etched with a) Nital 4% and b) modified Fry's reagent

The presence of different quantities of austenite between AM and CR sample is further demonstrated by the results of XRD analysis (Figure 3). AM samples are characterized by a volume fraction of austenite that is 6.1% higher than in the CR samples, probably because of differences in their chemical composition and heat treatments. It is expected that the solution treatment experienced by CR samples has promoted the dissolution of alloying elements, minimizing segregations, and obtaining a martensitic matrix after cooling. During the following aging treatment, the matrix can revert into the more stable reverse austenite. Instead, AM samples underwent only aging treatment, and in this case, austenite can be both retained, promoted by the presence of micro segregation, and reversed, deriving from the reversion of martensite during the aging holding (Jägge et al. 2014, Pereloma et al. 2004, Tan et al. 2017).

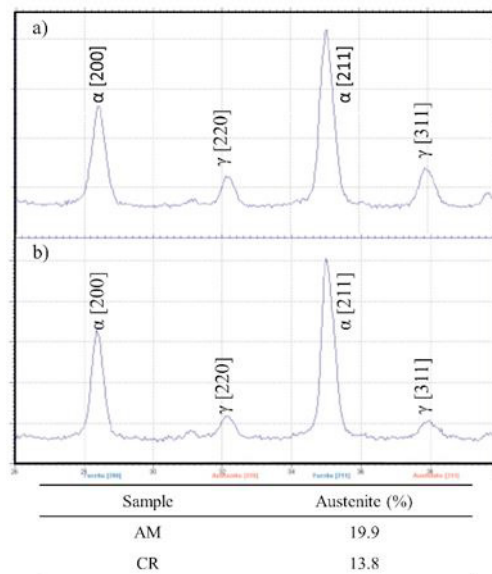


Figure 3 XRD analysis of samples a) AM and b) CR

The hardness of CR samples (54.6 ± 0.2 HRC) is about 1% higher than that of AM samples (53.9 ± 0.2 HRC). This small difference confirms that the heat treatment parameters were properly chosen. As suggested by other authors (Jägge et al. 2017), the slightly lower hardness of AM samples can be easily related to its highest content of soft austenite. Furthermore, hardness differences between AM and CR samples can also have other sources: different grain size, shape, density, and chemical composition of intermetallic precipitates (e.g. the lack of Ti in the AM alloy composition, contrary to the CR samples, results in the lack of Ni₃Ti nanoprecipitates).

Figure 4 displays the Coefficient of Friction (CoF) with the sliding distance, for wear tests carried out on both AM and CR samples with three different sliding velocities: 22.5, 50 and 62 cm/s. There are no relevant differences between the CoF measured on AM and CR samples. In particular, for all the tested conditions, the CoF values quickly reach a steady state that remains more stable at the slower sliding speed (Figure 4a), with respect to the velocity of 62 cm/s

(Figure 4c). Despite this difference, the average plateau values for the different samples remain very similar, close to 0.8, indicating that the sliding speed, in the considered range, has a negligible influence on the CoF.

Figure 4 Coefficient of Friction (CoF) Vs sliding distance as a function of sliding velocity a) 22.5 cm/s, b) 50 cm/s and c) 62 cm/s

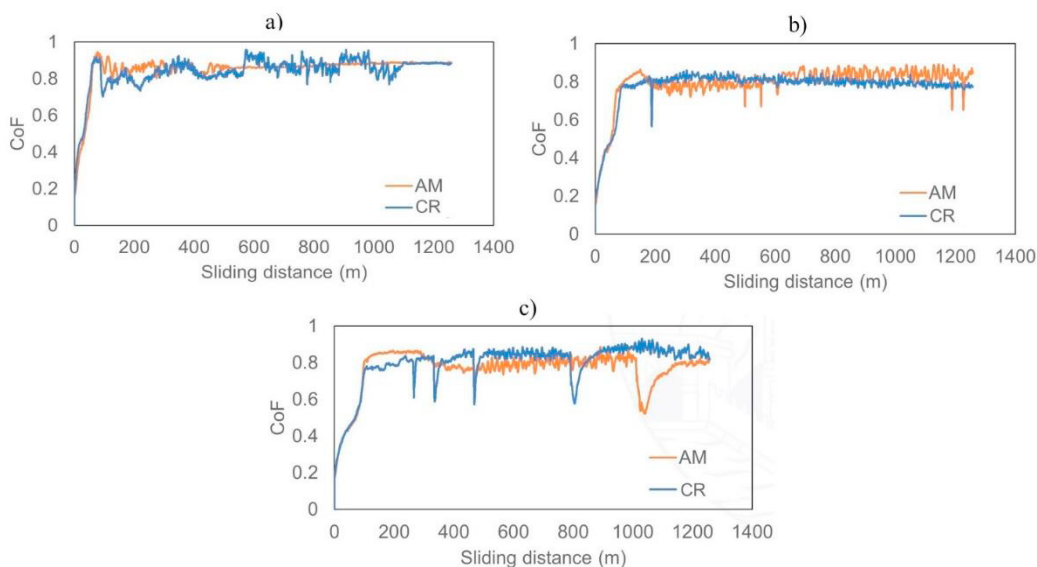


Figure 5 shows the samples wear rate (mm^3/Nm) at the end of each test for all the considered conditions. Notwithstanding the difference in their microstructure, the AM and CR samples show wear rates that are very similar for each velocity, suggesting that the hardness plays a more significant role in the wear behavior compared to the microstructural features of the samples. It can also be noted the increase in the wear rate with the sliding velocity, in accordance with the literature (Rai and Pathak 2004). In fact, the wear rate for the highest velocity results about 50% higher than for the tests carried out at 22.5 cm/s.

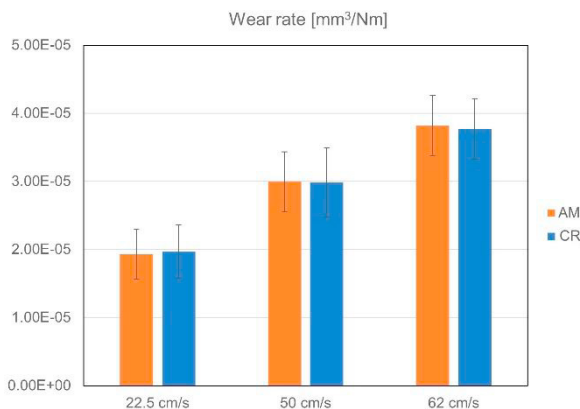


Figure 5 Wear rate ($\text{mm}^3 \text{N}^{-1} \text{m}^{-1}$) after 10000 laps of the tested samples

SEM analyses of the worn surfaces were carried out at the end of each test to investigate the wear mechanisms. These SEM images are presented in Figure 6. At the sliding velocity of 22.5 cm/s, both AM and CR samples show worn tracks with the presence of adhesion layers (Figure 6a and 6b), suggesting that the main wear mechanism is adhesion. Doubling the sliding speed from 22.5 to 50 cm/s, promotes the oxidation of the adhesive debris, embedded on the counterparts because the contact temperature is increased (Straffelini 2015), inducing two-body abrasion wear, as confirmed by the presence of ploughed grooves on the worn surfaces of both AM and CR samples (Figure 6c and 6d). A further increase of speed to 60 cm/s makes more evident this behavior, inducing the detachment of some embedded fragments from the steel ball and promoting a three-body abrasion mechanism. These oxidized wear

fragments rest on the worn surfaces in form of thick layers unevenly distributed. The worn surface areas free from fragments show evident signs of adhesive wear and still abrasive grooves (Figure 6e and 6f).

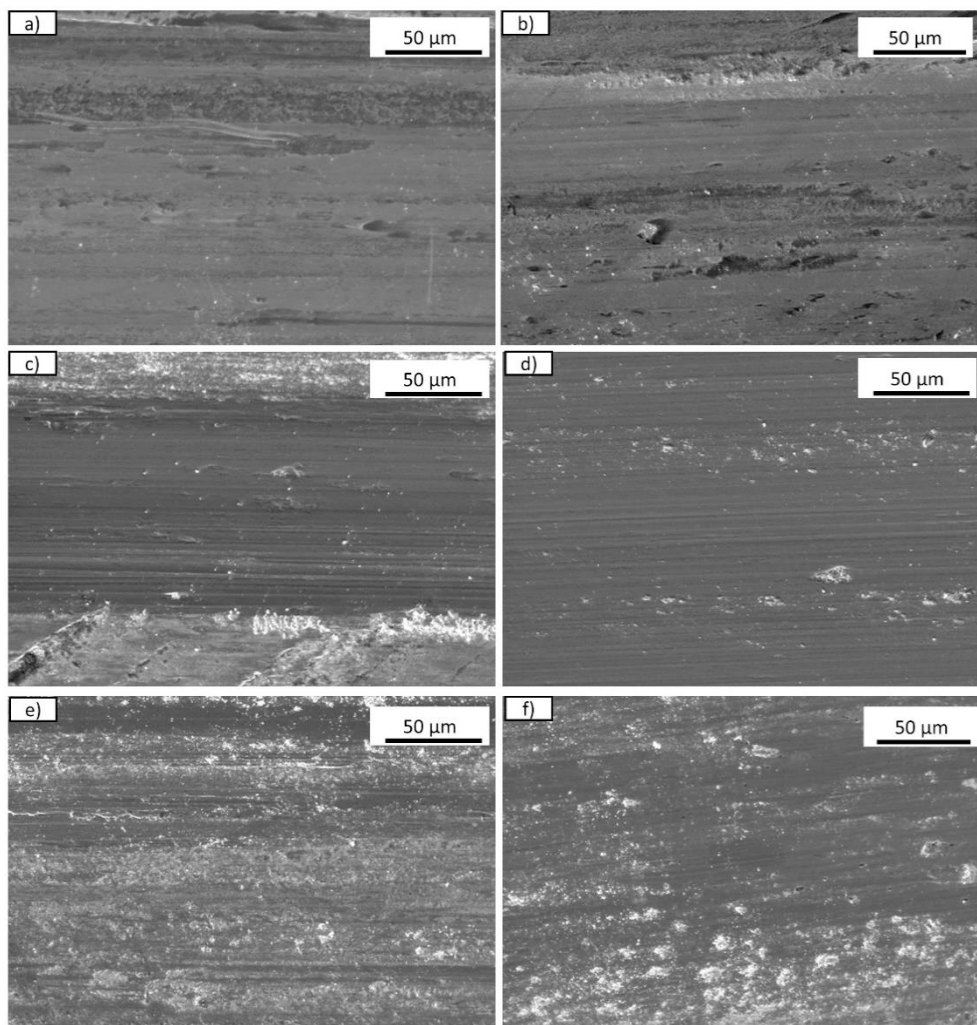


Figure 6 SEM images of wear tracks after 10000 laps for samples a) AM-22.5 cm/s b) CR-22.5 cm /s c) AM-50 cm/s d) CR-50 cm /s e) AM-62 cm/s and d) CR-62 cm /s

Finally, considering the result of corrosion tests, Figure 7 shows the plot of corrosion potential (V) versus corrosion current density (A/cm^2). The E_{corr} and I_{corr} values extrapolated from these plots with the Tafel method are summarized in Table 2. The results are in good agreement with data from literature (Suryawanshi *et al.* 2018). As can be noted, AM-horizontal and AM-vertical cross section exhibit a comparable corrosion behavior. Therefore, the anisotropy of the AM microstructure has a marginal role in the corrosion resistance to chlorine-bearing solutions. On the other hand, AM samples exhibit a nobler corrosion potential and a lower corrosion current density respect to the CR samples, indicating the better corrosion resistance of AM samples. This behavior can be related to the slightly different chemical composition between AM and CR samples. Furthermore, as reported in the literature (Khan *et al.* 2022), the finer microstructure typical of LPBF components is often related to their better corrosion resistance respect to wrought samples. Moreover, this difference can be also related to the highest austenite volume fraction of AM samples that normally is a phase nobler than the martensitic matrix (Mahmood Khan *et al.* 2022).

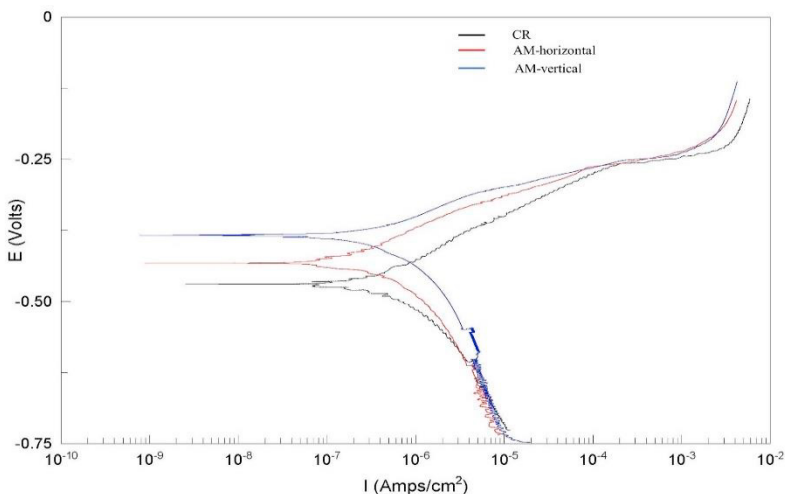
Figure 7 Potentiodynamic polarization tests results E_{corr} vs I_{corr}

Table 2 Average corrosion potential and corrosion current density values of the considered samples

Sample	E_{corr} (V)	I_{corr} ($\mu\text{A}/\text{cm}^2$)
AM-Vertical	-0.39	1.16
AM-Horizontal	-0.40	1.02
CR	-0.45	2.31

4. Conclusion

This work compares the sliding wear behavior and the corrosion resistance of 18Ni-300 maraging steel samples realized with two different manufacturing techniques: additive manufacturing and conventional forging route. The tests results showed that the AM components can compete with CR parts, notwithstanding the significant differences in microstructure deriving from the different production routes. In particular, the microstructure of AM parts is a fully dense fine cellular martensitic structure with the boundary of the melt pools and scan tracks clearly visible also after the aging treatment, while CR microstructure consist of blocks of lath type martensite, with a resulting hardness of 53.9 ± 0.2 HRC and 54.6 ± 0.2 HRC respectively. XRD measurements permitted also to verify that AM samples have austenite content 6% more than CR samples. Notwithstanding these differences, the results of the sliding wear tests are very similar for AM and CR samples, in terms of COF and wear rate, suggesting that the microstructure plays a minor role on the wear behavior that is dominated by materials hardness. In particular, the wear mechanism detected on the worn surfaces was mainly adhesive, with the tendency to turn in abrasive at the increasing of the sliding speed, with a consequent increase of wear rate.

About polarization corrosion tests in chloride-bearing solution, AM samples showed better resistance with respect to CR ones, displaying nobler corrosion potentials and lower corrosion current densities with respect to CR ones. Again, the microstructural anisotropy of AM samples seems to have only marginal effect on corrosion resistance, as the AM-vertical and AM-horizontal produced similar figures.

Acknowledgments

The authors would like to acknowledge MSc. Eng. A. Magistrelli of Bonomi Acciai for the preparation of the samples and Dr. D. Maestrini and Dr. G. Marconi of 2Effe Engineering for the support in the XRD analyses.

Reference

Aboulkhair, N. T., M. Simonelli, L. Parry, I. Ashcroft, C. Tuck & R. Hague (2019) 3D printing of Aluminium alloys: Additive Manufacturing of Aluminium alloys using selective laser melting. *Progress in Materials Science*, 106, 100578.

- Bai, Y., D. Wang, Y. Yang & H. Wang (2019) Effect of heat treatment on the microstructure and mechanical properties of maraging steel by selective laser melting. *Materials Science and Engineering: A*, 760, 105-117.
- Casati, R., J. N. Lemke, A. Tuissi & M. Vedani (2016) Aging Behaviour and Mechanical Performance of 18-Ni 300 Steel Processed by Selective Laser Melting. *Metals*, 6.
- E407, A. 2017. Standard Practice for Microetching Metals and Alloys. West Conshohocken, PA ASTM International.
- Elahinia, M., N. Shayesteh Moghaddam, M. Taheri Andani, A. Amerinatanzi, B. A. Bimber & R. F. Hamilton (2016) Fabrication of NiTi through additive manufacturing: A review. *Progress in Materials Science*, 83, 630-663.
- Ferreira, D. F. S., G. Miranda, F. J. Oliveira & J. M. Oliveira (2021) Predictive models for an optimized fabrication of 18Ni300 maraging steel for moulding and tooling by Selective Laser Melting. *Journal of Manufacturing Processes*, 70, 46-54.
- Giovagnoli, M., M. Tocci, A. Fortini, M. Merlin, M. Ferroni, A. Migliori & A. Pola (2021) Effect of different heat-treatment routes on the impact properties of an additively manufactured AlSi10Mg alloy. *Materials Science and Engineering: A*, 802, 140671.
- Handbook, A. 1993. *Properties and Selection: Irons, Steels, and High-Performance Alloys*.
- ISO/ASTM. 2019. ISO/ASTM 52911-1:2019, Additive manufacturing - Design - Part 1: Laser-based powder bed fusion of metals. West Conshohocken, PA: ASTM International.
- Jäggle, E. A., P.-P. Choi, J. Van Humbeeck & D. Raabe (2014) Precipitation and austenite reversion behavior of a maraging steel produced by selective laser melting. *Journal of Materials Research*, 29, 2072-2079.
- Jäggle, E. A., Z. Sheng, P. Kürnsteiner, S. Ocylok, A. Weisheit & D. Raabe (2017) Comparison of maraging steel micro- and nanostructure produced conventionally and by laser additive manufacturing. *Materials*, 10.
- Khan, H. M., G. Özer, M. S. Yilmaz & E. Koc (2022) Corrosion of Additively Manufactured Metallic Components: A Review. *Arabian Journal for Science and Engineering*, 47, 5465-5490.
- Kim, Y. G., G. S. Kim, C. S. Lee & D. N. Lee (1986) Microstructure and mechanical properties of a cobalt-free tungsten-bearing maraging steel. *Materials Science and Engineering*, 79, 133-140.
- Lang, F. H. & N. Kenyon (1971) Welding of maraging steels. *Welding Research Council Bulletin*.
- Liu, C., Z. Zhao, D. O. Northwood & Y. Liu (2001) A new empirical formula for the calculation of MS temperatures in pure iron and super-low carbon alloy steels. *Journal of Materials Processing Technology*, 113, 556-562.
- Mahmood Khan, H., G. Özer, M. Safa Yilmaz & G. Tarakci (2022) Improvement of Corrosion Resistance of Maraging Steel Manufactured by Selective Laser Melting Through Intercritical Heat Treatment. *Corrosion*, 78, 239-248.
- Morito, S., X. Huang, T. Furuhashi, T. Maki & N. Hansen (2006) The morphology and crystallography of lath martensite in alloy steels. *Acta Materialia*, 54, 5323-5331.
- Narayana Murty, S. V. S. & S. C. Sharma (2022) Materials for Indian Space Program: An Overview. *Journal of the Indian Institute of Science*, 102, 513-559.
- Pennings, B., K. Hatanaka & L. Crebolder. 2015. Improved properties of high strength 18Ni maraging steels for pushbelt CVT applications by optimization of alloy compositions and surface hardening heat treatments. In *European Conference on Heat Treatment 2015 and 22nd IFHTSE Congress - Heat Treatment and Surface Engineering from Tradition to Innovation*.
- Pereloma, E. V., A. Shekhter, M. K. Miller & S. P. Ringer (2004) Ageing behaviour of an Fe-20Ni-1.8Mn-1.6Ti-0.59Al (wt%) maraging alloy: clustering, precipitation and hardening. *Acta Materialia*, 52, 5589-5602.
- Rai, D. & J. P. Pathak (2004) Influence of sliding velocity on wear behaviour of different microstructures of Ni-Cr-Mo-V steel. *Indian Journal of Engineering and Materials Sciences*, 11, 113-120.
- Rao, M. N. (2006) Progress in understanding the metallurgy of 18% nickel maraging steels. *International Journal of Materials Research*, 97, 1594-1607.
- Schnitzer, R., M. Schober, S. Zinner & H. Leitner (2010) Effect of Cu on the evolution of precipitation in an Fe-Cr-Ni-Al-Ti maraging steel. *Acta Materialia - ACTA MATER*, 58, 3733-3741.
- Shin, J.-H., J. Jeong & J.-W. Lee (2015) Microstructural evolution and the variation of tensile behavior after aging heat treatment of precipitation hardened martensitic steel. *Materials Characterization*, 99, 230-237.
- Sing, S. L., J. An, W. Y. Yeong & F. E. Wiria (2016) Laser and electron-beam powder-bed additive manufacturing of metallic implants: A review on processes, materials and designs. *Journal of Orthopaedic Research*, 34, 369-385.
- Song, J., Q. Tang, Q. Feng, S. Ma, R. Setchi, Y. Liu, Q. Han, X. Fan & M. Zhang (2019) Effect of heat treatment on microstructure and mechanical behaviours of 18Ni-300 maraging steel manufactured by selective laser melting. *Optics & Laser Technology*, 120, 105725.
- Straffelini, G. 2015. *Friction and Wear*. Springer Cham.
- Suryawanshi, J., T. Baskaran, O. Prakash, S. B. Arya & U. Ramamurty (2018) On the corrosion resistance of some selective laser melted alloys. *Materialia*, 3, 153-161.
- Tan, C., K. Zhou, W. Ma, P. Zhang, M. Liu & T. Kuang (2017) Microstructural evolution, nanoprecipitation behavior and mechanical properties of selective laser melted high-performance grade 300 maraging steel. *Materials & Design*, 134, 23-34.
- Vasudevan, V. K., S. J. Kim & C. M. Wayman (1990) Precipitation reactions and strengthening behavior in 18 Wt Pct nickel maraging steels. *Metallurgical Transactions A*, 21, 2655-2668.
- Xu, X., S. Ganguly, J. Ding, S. Guo, S. Williams & F. Martina (2018) Microstructural evolution and mechanical properties of maraging steel produced by wire+arc additive manufacture process. *Materials Characterization*, 143, 152-162.
- Yin, S., C. Chen, X. Yan, X. Feng, R. Jenkins, P. O'Reilly, M. Liu, H. Li & R. Lupoi (2018) The influence of aging temperature and aging time on the mechanical and tribological properties of selective laser melted maraging 18Ni-300 steel. *Additive Manufacturing*, 22, 592-600.
- Zhang, L.-C. & H. Attar (2016) Selective Laser Melting of Titanium Alloys and Titanium Matrix Composites for Biomedical Applications: A Review. *Advanced Engineering Materials*, 18, 463-475.
- Zitelli, C., P. Folgarait & A. Di Schino (2019) Laser Powder Bed Fusion of Stainless Steel Grades: A Review. *Metals*, 9.